JOURNAL OF GEOPHYSICAL RESEARCH, VOL. 107, NO. B5, 10.1029/2001JB000264, 2002

Correction published 25 September 2002

Envelope broadening of spherically outgoing waves in three-dimensional random media having power law spectra

Tatsuhiko Saito, Haruo Sato, and Masakazu Ohtake

Department of Geophysics, Graduate School of Science, Tohoku University, Sendai, Japan

Received 5 September 2000; revised 30 May 2001; accepted 13 September 2001; published 9 May 2002.

[1] High-frequency *S* wave seismogram envelopes are broadened with increasing travel distance due to diffraction and scattering. The basic mechanism of the broadening has been studied on the basis of the scattering theory with the parabolic approximation for the scalar wave equation in random media. However, conventional models are not realistic enough since the plane wave modeling is too simple and the Gaussian autocorrelation function (ACF) is far from the reality to represent the inhomogeneity in the Earth. Focusing on the early part of envelopes, we formulated the envelope broadening of spherically outgoing scalar waves in three-dimensional von Kármán-type random media, of which the spectra decay according to a power law at large wave numbers. Random media are characterized by three parameters: RMS fractional velocity fluctuation ε, correlation distance a, and order κ that controls the gradient of the power law spectra. This model predicts that the envelope duration increases with both travel distance and frequency when short-wavelength components are rich in random media, while the duration is independent of frequency when short-wavelength components are poor. Introducing phenomenological attenuation Q, we developed a method for estimating the parameters of inhomogeneity and attenuation from the envelope duration. Applying this method to *S* wave seismogram envelopes for the frequency range from 2 to 32 Hz in northeastern Honshu Japan, we estimated the random inhomogeneity parameters as $\kappa = 0.6$, $\varepsilon^{2.2}a^{-1} \approx 10^{-3.6}$ [km^{-1}] and $f/Q = 0.0095$ [s^{-1}], where f is frequency. The power law portion of the estimated power spectral density function is $P(m) \approx 0.01\ m^{-4.2}$ [km^3], where m is wave number. *INDEX TERMS:* 7203 Seismology: Body wave propagation; 7218 Seismology: Lithosphere and upper mantle; 7260 Seismology: Theory and modeling; *KEYWORDS:* envelope, inhomogeneity, scattering, parabolic approximation, lithosphere

1. Introduction

[2] For the study of seismic wave propagation for frequencies higher than 1 Hz the velocity structure of the lithosphere cannot be simply modeled by horizontal layers. *Aki and Chouet* [1975] first showed that coda waves of local earthquakes are composed of scattered body waves by distributed scatterers in the lithosphere and that random inhomogeneity in elastic properties is the most probable origin of scattering. *Sato* [1989] proposed that the envelope broadening of *S* wave seismograms with increasing travel distance could be a powerful tool for the quantitative study of random velocity inhomogeneity in the lithosphere. For the incidence of scalar plane wave to random media extending in a half-space, *Lee and Jokipii* [1975] and *Sreenivasiah et al.* [1976] proposed a method to synthesize mean square (MS) envelope based on the Markov approximation for the parabolic wave equation when the random media is characterized by a Gaussian autocorrelation function (ACF) and the characteristic scale of inhomogeneity is much larger than the wavelength of incident waves. Their model predicts that diffraction and multiple forward scattering cause the envelope broadening. This Markov approximation method is an extension of the phase screen method for synthesizing waveforms to the stochastic synthesis of MS envelopes. Comparing the envelope simulation with the numerical waveform simulation based on the finite difference method, *Fehler et al.* [2000] recently confirmed the validity of both the Markov approximation method and the phase screen method for the synthesis of waveforms except latter coda in two-dimensional random media characterized by a Gaussian ACF. Introducing an attenuation factor in the Markov approximation method, *Sato* [1989] and *Scherbaum and Sato* [1991] quantitatively estimated the ACF of random velocity inhomogeneity in the lithosphere beneath the Kanto region, Japan, from the envelope analysis of small-earthquake records. Their simulations can basically explain the envelope-broadening phenomenon. However, if we apply the above scattering model to observed seismogram envelopes, it is better to use not plane waves but spherical waves. Therefore we need to develop mathematics for modeling envelope of spherically outgoing waves radiated from a point source.

[3] Analyzing seismic coda waves, *Wu and Aki* [1985] found that the spectral characteristics of velocity fluctuation obey a power law. In order to explain the frequency dependence of *S* wave attenuation and coda excitation, *Sato* [1990] proposed a scattering-loss model to use the von Kármán-type ACF for describing the random inhomogeneity which has power law spectra at large wave numbers. The spectral structure of random inhomogeneity was also studied by the correlation analysis of teleseismic waves based on the parabolic approximation for scalar wave equation [*Aki*, 1973; *Capon*, 1974]. *Flatté and Wu* [1988] developed this method and analyzed seismic array data at NORSAR. They proposed a two-overlapping-layer model that has power law spectra. *Gusev and Abubakirov* [1996] simulated not only coda part but also full envelopes in random media by using the Monte Carlo simulation method based on the radiative transfer theory with a scattering coefficient derived from the Born approximation. They concluded that simulated envelopes qualitatively well explain observed seismogram envelopes when the PSDF has power law spectra with its power being -3.5 to -4 for large wave numbers. *Shiomi et al.*

0148-0227/02/2001JB000264$09.00

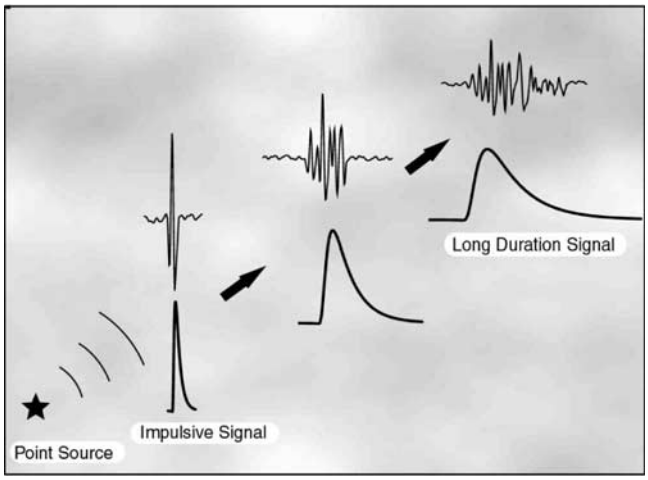

Figure 1. Schematic illustration of spherically outgoing waves radiated from a point source and their envelopes in a randomly inhomogeneous medium. Waves, which are impulsive at the source radiation, are distorted, and the duration gets longer with increasing propagation distance.

[1997] reported that the small-scale inhomogeneity in the shallow crust is random by examining elastic wave velocities and density from well log data at various sites. They concluded that its power spectral density function (PSDF) has power law spectra. From these studies we get to know that the velocity inhomogeneity of the real earth medium is random in space and its statistical character is well represented by PSDF having power law spectra. For the simulation of envelopes, *Obara and Sato* [1995] introduced an exponential-like function for the longitudinal integral of ACF and attempted to explain the frequency dependence of envelope broadening characteristics observed in Kanto-Tokai area in Japan, but the corresponding ACF was not mathematically defined yet. Therefore we need to develop mathematics to synthesize envelopes in random media of which the PSDF has power law spectra. The von Kármán-type ACF is one of the simplest functions that have power law spectra at large wave numbers.

[4] In this paper, we develop mathematics to simulate the envelope of spherically outgoing scalar waves radiated from a point source in three-dimensional (3-D) random media that are characterized by the von Kármán-type ACF. *Shishov* [1974] solved a similar problem, but his result is limited to the case of Gaussian ACF only. On the basis of this new model we propose a method to estimate the PSDF characterizing the random inhomogeneity and the attenuation factor from the travel distance dependence and the frequency dependence of envelope broadening. As an application of this method, we quantitatively estimate the PSDF of random velocity inhomogeneity of the lithosphere beneath northeastern Honshu, Japan, from the analysis of *S* wave seismogram envelopes of small earthquakes recorded at a single station.

2. Envelope Synthesis in Random Media

[5] We imagine that waves radiated from a point source spherically propagate through a 3-D inhomogeneous medium as schematically illustrated in Figure 1. Velocity inhomogeneities cause scattering and diffraction effects on the waves. As a result, waves, which are impulsive at the source, are distorted, and the duration gets longer as the propagation distance increases. Here we focus on the envelope broadening phenomenon and study mathematically the physical mechanism. The wave velocity inhomogeneity is written as $V(\mathbf{x}) = V_0\{1 + \xi(\mathbf{x})\}$, where V_0 is the background velocity and fractional fluctuation $\xi(\mathbf{x})$ is a spatially random function. We introduce an ensemble of random function $\{\xi(\mathbf{x})\}$, where $\langle\xi(\mathbf{x})\rangle = 0$. The angle brackets indicate the ensemble average. We assume that the randomness is statistically homogeneous and isotropic. The random media can be characterized by the ACF of fractional velocity fluctuation $R(\mathbf{x}) \equiv \langle\xi(\mathbf{x}+\mathbf{x}')\,\xi(\mathbf{x}')\rangle$. The magnitude of inhomogeneity is given by the MS fractional fluctuation $\varepsilon^2 \equiv R(0) = \langle\xi(0)^2\rangle$, and the characteristic scale is given by the correlation distance a.

2.1. Markov Approximation for the Parabolic Wave Equation

[6] We assume that the wavelength $\lambda(= 2\pi/k)$ is shorter than the correlation distance a of the random inhomogeneity ($ak \gg 1$), where k is the wave number. Neglecting conversion scattering between *P* and *S* waves in such a case, it is justified to describe the principal characteristics of elastic wave propagation by using the wave equation for scalar wave field $u(\mathbf{x}, t)$:

$$\left(\Delta - \frac{1}{V(\mathbf{x})^2}\frac{\partial^2}{\partial t^2}\right)u(\mathbf{x},t) = 0, \tag{1}$$

where Δ is Laplacian. When the fractional velocity fluctuation is small, $|\xi(\mathbf{x})| \ll 1$, the wave equation (1) is written as

$$\left(\Delta - \frac{1}{V_0^2}\frac{\partial^2}{\partial t^2}\right)u(\mathbf{x},t) + \frac{2}{V_0^2}\xi(\mathbf{x})\frac{\partial^2}{\partial t^2}u(\mathbf{x},t) = 0. \tag{2}$$

We study the propagation of spherically outgoing waves radiated from a point source located at the origin. Therefore we introduce polar coordinates (r, θ, ϕ), where angle θ is measured from the direction of a receiver. We may write the scalar wave field as a superposition of harmonic spherical waves of angular frequency ω as

$$u(\mathbf{x},t) = \frac{1}{2\pi}\int_{-\infty}^{\infty}\frac{U(r,\theta,\phi,\omega)}{r}e^{i(kr-\omega t)}d\omega, \tag{3}$$

where $k = \omega/V_0$ and $r = |\mathbf{x}|$. The Laplacian in (2) is written as

$$\Delta = \frac{1}{r^2}\frac{\partial}{\partial r}\left(r^2\frac{\partial}{\partial r}\right) + \frac{1}{r^2}\Delta_\perp, \tag{4}$$

where the angular part of Laplacian $\Delta_\perp$ is given by

$$\Delta_\perp = \frac{1}{\sin\theta}\frac{\partial}{\partial\theta}\left(\sin\theta\frac{\partial}{\partial\theta}\right) + \frac{1}{\sin^2\theta}\frac{\partial^2}{\partial\phi^2}. \tag{5}$$

When $ak \gg 1$, substituting equations (3) and (4) into (2) and neglecting the second derivative with respect to r, we obtain the parabolic wave equation:

$$2ik\frac{\partial}{\partial r}U(r,\theta,\phi,\omega) + \frac{1}{r^2}\Delta_\perp U(r,\theta,\phi,\omega) - 2k^2\xi(r,\theta,\phi)U(r,\theta,\phi,\omega) = 0. \tag{6}$$

The parabolic approximation neglecting large-angle scattering is considered to be applicable only when the medium has poor short-wavelength components. However, the parabolic wave equation would be able to predict at least early part of waveforms quantitatively even when random media have rich short-wavelength components because the early part is mainly

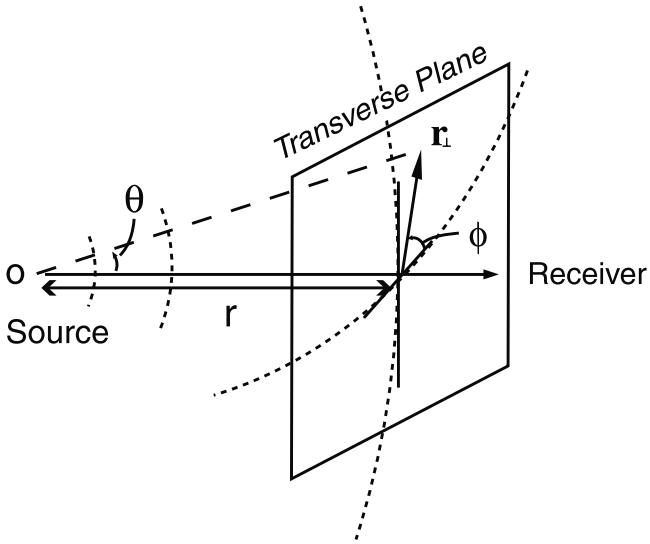

Figure 2. At a large distance r from the source ($r \gg a$) we take the local Cartesian coordinates in a small volume, where the one axis is in the direction of a receiver and the other two axes are in the transverse plane which is tangent to the sphere of radius r. Angle θ is measured from the receiver direction.

composed of waves scattered within narrow angles around the receiver direction. By comparing waveforms numerically calculated from the wave equation and those from the parabolic wave equation, *Liu and Wu* [1994] confirmed the validity of the parabolic approximation in von Kármán-type random media with the order of 0.5 and in flicker-noise random media when the fractional velocity fluctuation is <10%.

[7] For the case of $ak \gg 1$, small-angle scattering dominates. Therefore we use the local Cartesian coordinate system in a small volume at a large distance r from the source ($r \gg a$), where one axis is chosen to be in the receiver direction and the other two axes are in the transverse plane which is tangent to the sphere of radius r (see Figure 2). According to *Ishimaru* [1978] we define the two-frequency mutual coherence function (TMCF) on the transverse plane at distance r, which means the correlation between different locations $\mathbf{r}_{\perp 1}$ and $\mathbf{r}_{\perp 2}$ on the transverse plane and different angular frequencies ω_1 and ω_2,

$$\Gamma_2(\mathbf{r}_{\perp 1}, \mathbf{r}_{\perp 2}, r, \omega_1, \omega_2) \equiv \langle U(r, \mathbf{r}_{\perp 1}, \omega_1) U^*(r, \mathbf{r}_{\perp 2}, \omega_2) \rangle, \quad (7)$$

where the asterisk indicates complex conjugate. Since the random media are statistically homogeneous, Γ_2 depends only on the difference between $\mathbf{r}_{\perp 1}$ and $\mathbf{r}_{\perp 2}$. For quasi-monochromatic waves, that is, $\omega_1 \approx \omega_2$, we can get the master equation for Γ_2 from (6) as

$$\frac{\partial}{\partial r}\Gamma_2 + i\frac{k_d}{2k_c^2}\frac{1}{r^2}\left(\frac{\partial^2}{\partial \theta_d^2} + \frac{1}{\theta_d}\frac{\partial}{\partial \theta_d}\right)\Gamma_2 + k_c^2[A(0) - A(r\theta_d)]\Gamma_2 + \frac{k_d^2}{2}A(0)\Gamma_2 = 0, \quad (8)$$

where the difference transverse coordinate is defined as $\mathbf{r}_{\perp d} \equiv \mathbf{r}_{\perp 1} - \mathbf{r}_{\perp 2}$ and the difference angle is defined as $\theta_d \equiv |\mathbf{r}_{\perp d}|/r$. The derivation is given in Appendix A. Note that we assume no backscattering. This derivation is called the Markov approximation [*Tatarskii*, 1971]. This approximation puts a focus on strong forward scattering and diffraction effect. We introduce the center of mass and difference coordinates in the wave number space as $k_c = (k_1 + k_2)/2$ and $k_d = k_1 - k_2$ ($k_d \ll k_c$), respectively. Corresponding coordinates for angular frequency will also be used. The effect of inhomogeneity is included in the longitudinal integral of ACF:

$$A(r_{\perp d}) = A(\mathbf{r}_{\perp d}) \equiv \int_{-\infty}^{\infty} dz R(\mathbf{r}_{\perp d}, z), \quad (9)$$

where z is the radial coordinate in ACF and $r_{\perp d} = |\mathbf{r}_{\perp d}|$. The last term in (8) does not affect the broadening of individual wave packets but shows the wandering effect, which is the travel time fluctuation over different rays for each element of ensemble [*Lee*

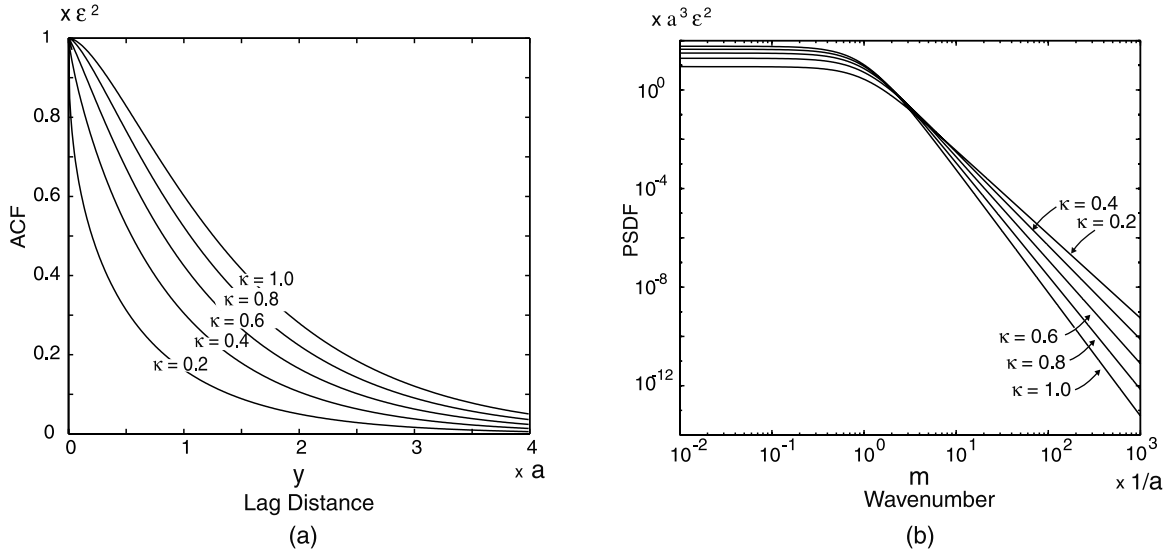

Figure 3. Plots of (a) von Kármán-type autocorrelation function and (b) the corresponding power spectral density function for different values of order κ. The power spectral density function decays according to a power law $m^{-2\kappa-3}$ for large wave number.

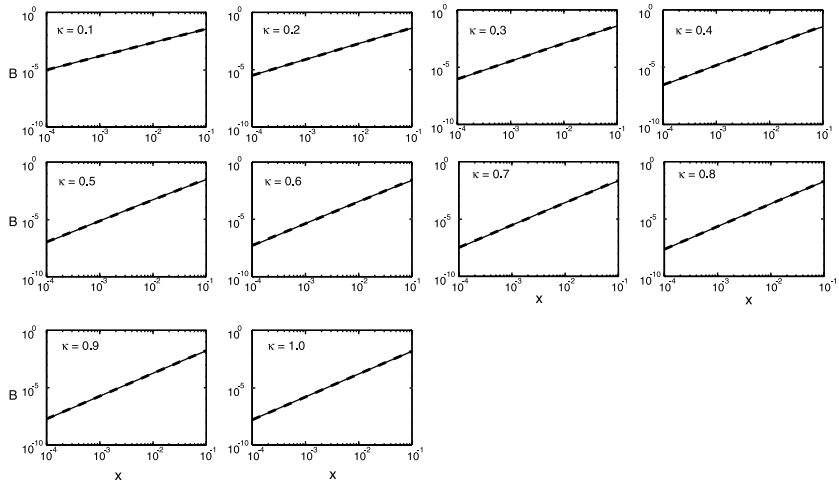

Figure 4. Comparison between the function $B(x)$ given by equation (19) (solid curve) and its approximation form given by equation (20) (dashed line) for various κ values for $10^{-4} < x < 10^{-1}$. Coefficients used in the approximation form are listed in Table 1.

and Jokipii, 1975]. Therefore, removing the last term, we get the master equation as

$$\frac{\partial}{\partial r}{}_0\Gamma_2 + i\frac{k_d}{2k_c^2}\frac{1}{r^2}\left(\frac{\partial^2}{\partial\theta_d^2}+\frac{1}{\theta_d}\frac{\partial}{\partial\theta_d}\right){}_0\Gamma_2 + k_c^2[A(0)-A(r\theta_d)]{}_0\Gamma_2 = 0, \tag{10}$$

where we use the symbol ${}_0\Gamma_2$ instead of Γ_2 in the following. Equation (10) corresponds to equation (8) of *Shishov* [1974]. The above derivation is analogous to that for plane waves [*Ishimaru*, 1978; *Sato*, 1989; *Sato and Fehler*, 1998].

[8] We define the intensity of waves at radial distance r and lapse time t as an ensemble average of wave's power:

$$\begin{aligned} I_0(r,t) &\equiv \langle u(r,\mathbf{r}_\perp,t)u^*(r,\mathbf{r}_\perp,t)\rangle \\ &= \frac{1}{(2\pi)^2}\frac{1}{r^2}\int_{-\infty}^{\infty}\int_{\infty} d\omega_d d\omega_c \\ &\cdot {}_0\Gamma_2(\theta = {}_d0, r, \omega_d, \omega_c)e^{-i\omega_d(t-r/V_0)} \\ &= \frac{1}{2\pi}\int_{-\infty}^{\infty} d\omega_c \hat{I}_0(r,t;\omega_c). \end{aligned} \tag{11}$$

Table 1. $C(\kappa)$ and $p(\kappa)$ in Equation (20) Estimated for $10^{-4} < x < 10^{-1}$

κ	$C(\kappa)$	$p(\kappa)$
0.1	0.56	1.19
0.2	1.06	1.38
0.3	1.56	1.56
0.4	2.00	1.71
0.5	2.28	1.83
0.6	2.31	1.91
0.7	2.14	1.95
0.8	1.90	1.98
0.9	1.68	1.99
1.0	1.50	1.99

The intensity spectral density (ISD) $\hat{I}_0$ is written as the inverse Fourier transform of the TMCF with respect to difference angular frequency:

$$\hat{I}_0(r,t;\omega_c) = \frac{1}{2\pi r^2}\int_{-\infty}^{\infty} {}_0\Gamma_2(\theta_d = 0, r, \omega_d, \omega_c)e^{-i\omega_d(t-r/V_0)}d\omega_d. \tag{12}$$

It corresponds to the mean square of a band-pass-filtered trace having center angular-frequency ω_c, that is, the MS envelope. Its square root gives the RMS envelope. When we take ${}_0\Gamma_2$ to be nondimensional for a unit source radiation,

$${}_0\Gamma_2(\theta_d, r = 0, \omega_d, \omega_c) = 1/4\pi, \tag{13}$$

as the initial condition for coherent isotropic radiation from the point source, the ISD has a dimension of flux density and satisfies

$$\hat{I}_0(r\to 0, t;\omega_c) = \frac{1}{4\pi r^2}\delta\left(t-\frac{r}{V_0}\right). \tag{14}$$

2.2. MS Envelopes in von Kármán-Type Random Media

2.2.1. The von Kármán-type random media. [9] A von Kármán-type ACF (Figure 3a) is given by

$$R(\mathbf{y}) = R(y) = \frac{\varepsilon^2 2^{1-\kappa}}{\Gamma(\kappa)}\left(\frac{y}{a}\right)^{\kappa}K_\kappa\left(\frac{y}{a}\right), \tag{15}$$

where $y = |\mathbf{y}|$, Γ is the gamma function and K_κ is the modified Bessel function of the second kind of order κ. The corresponding PSDF (Figure 3b) is

$$\begin{aligned} P(\mathbf{m}) = P(m) &= \frac{8\pi^{\frac{3}{2}}\varepsilon^2 a^3\Gamma\left(\kappa+\frac{3}{2}\right)}{\Gamma(\kappa)(1+a^2m^2)^{\kappa+\frac{3}{2}}} \\ &\approx \frac{8\pi^{\frac{3}{2}}\Gamma\left(\kappa+\frac{3}{2}\right)\left(\frac{\varepsilon^{1/\kappa}}{a}\right)^{2\kappa}}{\Gamma(\kappa)}m^{-2\kappa-3} \qquad am \gg 1. \end{aligned} \tag{16}$$

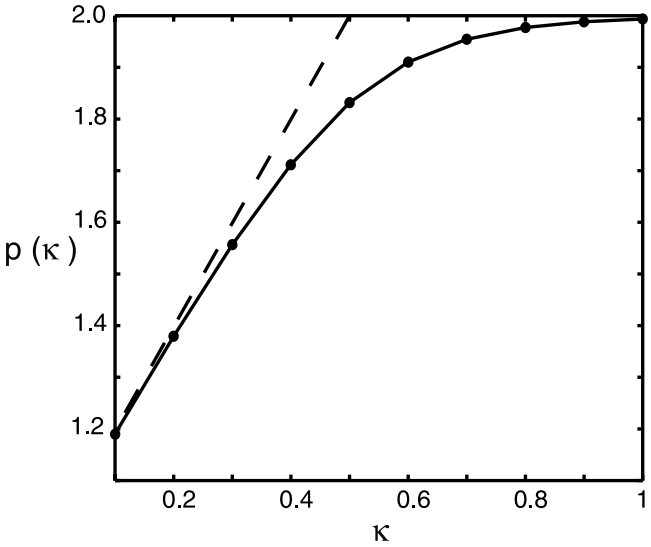

Figure 5. Plots of power index $p(\kappa)$ against κ for $10^{-4} < x < 10^{-1}$. Dashed line shows the asymptote $2\kappa + 1$ for $\kappa \ll 0.5$. The asymptotic value for $\kappa \gg 0.5$ is 2.

The PSDF obeys the power law for large wave numbers, and the power is given by $-2\kappa - 3$. It means that short-wavelength components of random media increase with decreasing the order κ. In this study, we restrict the range of κ to be between 0 and 1.

2.2.2. ISD for the von Kármán-type random media. [10] For the von Kármán-type random media we can calculate the longitudinal integral of ACF A (see equation (9)) from the PSDF as

$$A(\mathbf{r}_{\perp d}) = \int_{-\infty}^{\infty} dz \frac{1}{(2\pi)^3} \int \int_{-\infty}^{\infty} \int P(\mathbf{m}) e^{i\mathbf{m}(r_{\perp d} + z e_z)} d\,\mathbf{m}$$

$$= \frac{2^{-\kappa+3/2}\sqrt{\pi}\,\varepsilon^2 a}{\Gamma(\kappa)} \left(\frac{r_{\perp d}}{a}\right)^{\kappa+1/2} K_{\kappa+1/2}\left(\frac{r_{\perp d}}{a}\right), \tag{17}$$

by using integral formulas [*Abramowitz and Stegun*, 1970]. Then we need to get the representation of difference $A(0) - A(r\,\theta_d)$ appearing in equation (10). We may write that as

$$A(0) - A(r\,\theta_d) = \varepsilon^2 a\, B\left(\frac{r\,\theta_d}{a}; \kappa\right), \tag{18}$$

where

$$B(x;\kappa) \equiv \frac{2^{-\kappa+\frac{3}{2}}\sqrt{\pi}}{\Gamma(\kappa)} \left[\lim_{x\to 0}\left(x^{\kappa+\frac{1}{2}} K_{\kappa+\frac{1}{2}}(x)\right) - x^{\kappa+\frac{1}{2}} K_{\kappa+\frac{1}{2}}(x)\right]. \tag{19}$$

At a long travel distance from the source the correlation of wave field at two points spatially separated on a transverse plane rapidly decreases to zero with increasing lag distance [*Sato and Fehler*, 1998], and as a result, ${}_0\Gamma_2$ gets close to zero with increasing lag distance. Therefore the contribution from a small transverse distance $r_{\perp d} \ll a$ is dominant. That is, the contribution of $B(x;\kappa)$ for $x \ll 1$ is important. We may approximate as

$$B(x;\kappa) \approx C(\kappa) x^{p(\kappa)} \qquad x \ll 1. \tag{20}$$

Using an expansion formula for $B(x;\kappa)$ given by equation (19) [*Abramowitz and Stegun*, 1970], except for $\kappa = 1/2$, we get the approximation form as

$$B(x;\kappa) \approx \frac{2^{-\kappa+\frac{1}{2}}\pi^{\frac{3}{2}}}{\Gamma(\kappa)\cos\kappa\pi} \left\{ -\frac{2^{\kappa-\frac{3}{2}}}{\Gamma\left(\frac{3}{2}-\kappa\right)} x^2 + \frac{2^{-\kappa-\frac{1}{2}}}{\Gamma\left(\frac{3}{2}+\kappa\right)} x^{2\kappa+1} \right\} \quad x \ll 1. \tag{21}$$

For the case of $\kappa \gg 1/2$ and the case of $\kappa \ll 1/2$, the leading term in equation (21) is dominant:

$$B\left(\frac{r_{\perp d}}{a}; \kappa\right) \approx \frac{2^{-\kappa+\frac{1}{2}}\pi^{\frac{3}{2}}}{\Gamma(\kappa)\cos\kappa\pi} \left\{ \frac{-2^{-\kappa-\frac{1}{2}}}{\Gamma(3/2+\kappa)} \left(\frac{r_{\perp d}}{a}\right)^{2\kappa+1} \right\} \tag{22a}$$

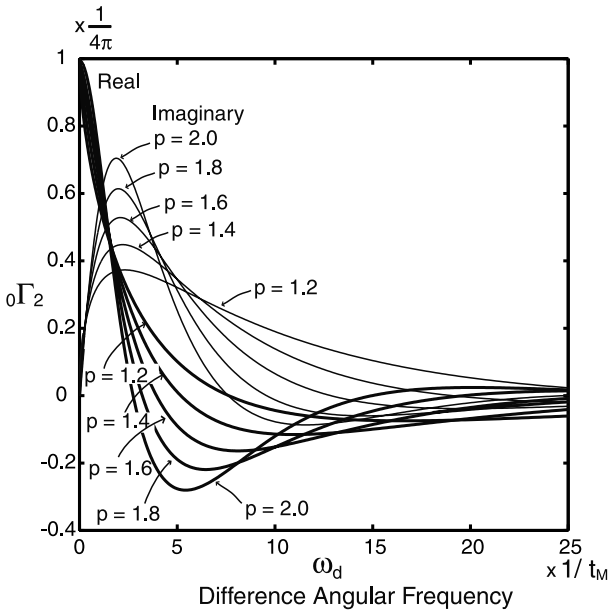

Figure 6. Plots of real and imaginary parts of ${}_0\Gamma_2$ against difference angular frequency numerically calculated for different p values.

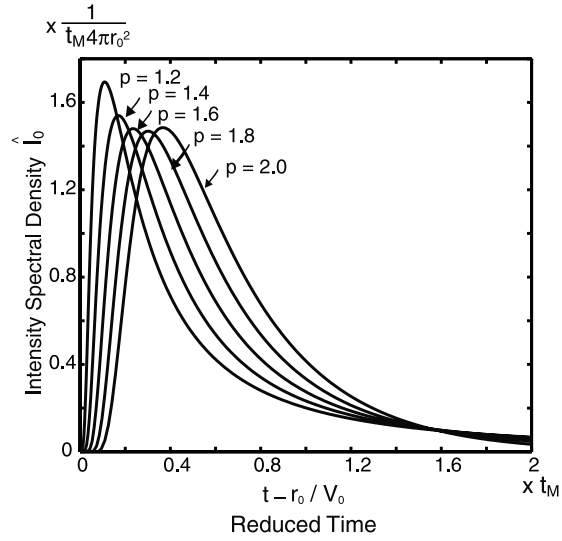

Figure 7. Temporal change in ISD calculated numerically for different p values.

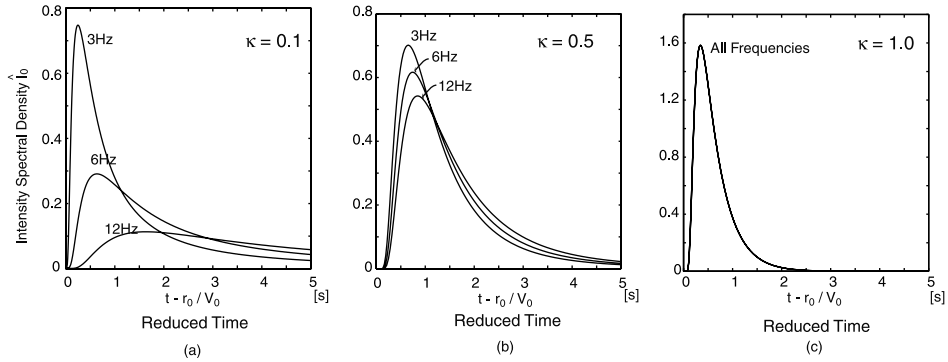

Figure 8. Temporal change in ISD for three different frequencies at a distance r_0 = 100 km for von Kármán-type random media without attenuation. High-frequency envelopes are more broaden than low-frequency ones in the case of $\kappa = 0.1$ and $\kappa = 0.5$. For $\kappa = 0.1$, envelope becomes independent of frequency.

for $\kappa \ll 1/2$, and

$$B\left(\frac{r_{\perp d}}{a};\kappa\right) \approx \frac{2^{-\kappa+\frac{1}{2}}\pi^{\frac{3}{2}}}{\Gamma(\kappa)\cos\kappa\pi}\left\{\frac{2^{\kappa-\frac{3}{2}}}{\Gamma(3/2-\kappa)}\left(\frac{r_{\perp d}}{a}\right)^2\right\} \tag{22b}$$

for $\kappa \gg 1/2$. Thus we get to know the asymptotical behavior of B for $x \ll 1$ in the cases of small and large κ values.

[11] These asymptotic solutions, however, are not available when κ is close to 1/2, so that we take advantage of numerical evaluation. Varying κ from 0.1 to 1.0 by 0.1 step in equation (19), we numerically estimate $p(\kappa)$ and $C(\kappa)$ in equation (20). In Figure 4 the approximation form (equation (20)) is plotted by a dashed line together with its original form (equation (19)) by a solid line for the x range from 10^{-4} to 10^{-1} in logarithmic scale for different κ values. For the corresponding x range, we can approximate the function $B(x;\kappa)$ within 15% error. The estimated $p(\kappa)$ and $C(\kappa)$ are listed in Table 1. Plot of $p(\kappa)$ against κ is given in Figure 5. Value $p(\kappa)$ increases and the gradient decreases as κ increases. At $\kappa = 0.1$ and 1.0, $p(\kappa)$ is nearly 1.2 and 2.0, respectively, as predicted by analytical asymptotic solutions.

[12] Substituting equations (18) and (20) into (10), we get

$$\frac{\partial}{\partial r^0}\Gamma_2 + i\frac{k_d}{2k_c^2}\frac{1}{r^2}\left(\frac{\partial^2}{\partial\theta_d^2}+\frac{1}{\theta_d}\frac{\partial}{\partial\theta_d}\right){}_0\Gamma_2 + k_c^2\varepsilon^2 aC(\kappa)\left(\frac{r\theta_d}{a}\right)^p{}_0\Gamma_2 = 0. \tag{23}$$

We define the characteristic time as

$$t_M = \frac{C(\kappa)^{\frac{2}{p}}\varepsilon^{\frac{4}{p}}a}{2V_0}\left(\frac{a\omega}{V_0}\right)^{\frac{-2p+4}{p}}\left(\frac{r_0}{a}\right)^{\frac{p+2}{p}} = \frac{C(\kappa)^{\frac{2}{p}}V_0^{\frac{p-4}{p}}}{2}\left(\varepsilon^{\frac{1}{p-1}}a^{-1}\right)^{\frac{2p-2}{p}}\omega^{\frac{-2p+4}{p}}r_0^{\frac{p+2}{p}}, \tag{24}$$

and the nondimensional propagation distance τ and the transverse distance χ as

$$\tau = r/r_0, \qquad \chi = \sqrt{2r_0V_0k_c^2t_M}\,\theta_d. \tag{25}$$

Using equations (24) and (25), we may write (23) in nondimensional form as

$$\frac{\partial}{\partial\tau}{}_0\Gamma_2 + it_M\omega_d\frac{1}{\tau^2}\left(\frac{\partial^2}{\partial\chi^2}+\frac{1}{\chi}\frac{\partial}{\partial\chi}\right){}_0\Gamma_2 + \tau^p\chi^p{}_0\Gamma_2 = 0. \tag{26}$$

Additionally, introducing new parameters μ and ν as

$$\mu = (t_M\omega_d)^{p/(p+2)}\tau \qquad \nu = (t_M\omega_d)^{-(p+1)/(p+2)}\chi, \tag{27}$$

we rewrite equation (26) as

$$\frac{\partial}{\partial\mu}{}_0\Gamma_2 + i\frac{1}{\mu^2}\left(\frac{\partial^2}{\partial\nu^2}+\frac{1}{\nu}\frac{\partial}{\partial\nu}\right){}_0\Gamma_2 + \mu^p\nu^p{}_0\Gamma_2 = 0. \tag{28}$$

For the case $p = 2$, we can get an analytical solution of equation (26). Substituting the solution into equation (12), we get analytical solution for ISD at a distance r_0 as

$$\hat{I}_0(r_0,t) = \frac{1}{4\pi r_0^2}H\left(t-\frac{r_0}{V_0}\right)\frac{\pi^2}{2t_M}\cdot\sum_{n=1}^{\infty}(-1)^{n+1}n^2\exp\left[-\frac{n^2\pi^2(t-r_0/V_0)}{4t_M}\right] \tag{29}$$

for $p = 2$, where $H(t)$ is a step function. Representation (29) is the same as the solution for random media characterized by a Gaussian ACF, except for the definition of characteristic time,

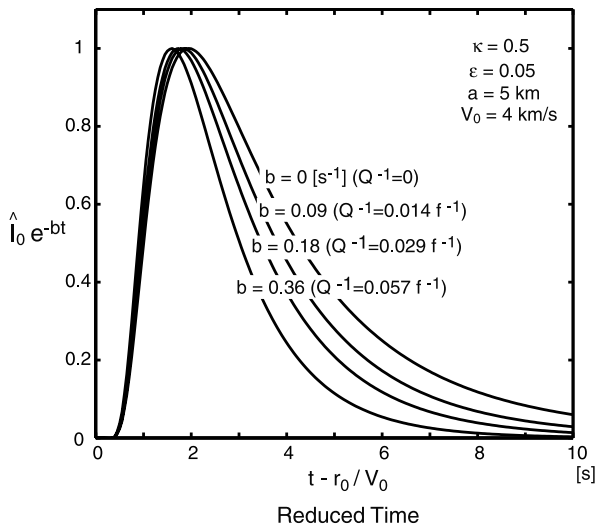

Figure 9. Temporal change in ISD at r_0 = 150 km at the 6 Hz band for different values of b in the presence of attenuation. Each trace is normalized by the maximum amplitude.

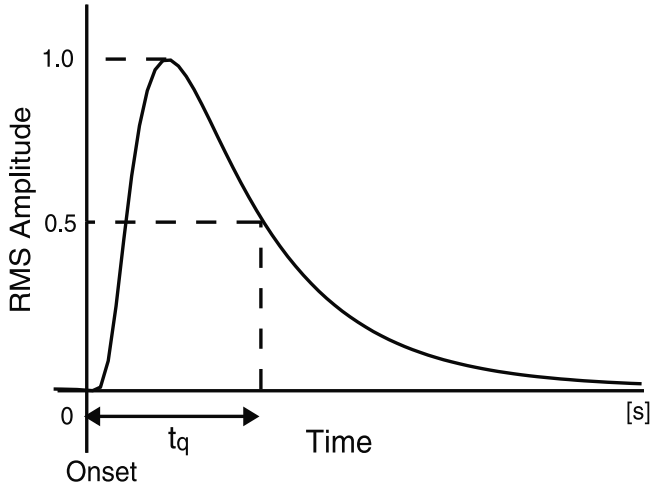

Figure 10. Duration t_q is defined as the time lag between the onset and the time when the root-mean-square (RMS) envelope decays to the half of the maximum value.

which was originally solved by *Shishov* [1974] (see Appendix B). For the case $p \neq 2$ it is difficult to solve equation (28) analytically. We can numerically solve equation (28) under the initial condition ${}_0\Gamma_2(\nu, \mu = 0) = 1/4\pi$. We use the Crank-Nicholson method [*Press et al.*, 1987], where μ is developed by 0.01 step and the interval in the ν space (0, 10) is divided into 600 segments. Then we transform ${}_0\Gamma_2(\nu, \mu)$ into ${}_0\Gamma_2(\chi,\tau; t_M\omega_d)$. Figure 6 shows resultant ${}_0\Gamma_2(\chi = 0, \tau = 1; t_M\omega_d)$ for various p values. We numerically simulate the ISD for different p values using the Fourier transform of ${}_0\Gamma_2$ with respect to $t_M\omega_d$. Synthesized ISDs for various p values are illustrated in Figure 7 after the correction of geometrical spreading. Reduced time $t - r_0/V_0$ is scaled by characteristic time t_M. We see that envelope "shape" for larger p has apparently longer duration in the scaled time in Figure 7 but note that we need to take not only envelope shape but also characteristic time t_M (equation (24)) into account when we evaluate envelope duration in time.

2.2.3. Travel distance dependence and wave frequency dependence of ISD. [13] In the definition of characteristic time (see equation (24)) the power of travel distance is $1 + 2/p$, and p increases with κ (see Figure 5). It means that the travel distance dependence of the ISD is strong when the inhomogeneity spectra have rich short-wavelength components (small κ), while the dependence is weak when the spectra have poor short-wavelength components (large κ). The power of angular frequency is $-2 + 4/p$. This means that there is no frequency dependence of ISD for the case $p = 2$, that is, poor in short-wavelength component ($\kappa \approx 1.0$). On the other hand, the frequency dependence increases as short-wavelength components of random media increase (κ or p value decreases). As an example, Figure 8 shows the frequency dependence of the ISD at $r_0 = 100$ km for various κ values, where $\varepsilon = 0.05$, $a = 5$ km, $V_0 = 4$ km/s. For random media with $\kappa = 0.1$ the envelope strongly depends on frequency. High-frequency envelopes are more broaden than low-frequency ones. For random media with $\kappa = 0.5$, which have less short-wavelength components, the frequency dependence becomes weak, and for $\kappa = 1.0$ the envelope is independent of frequency. Previous studies [*Sato*, 1989; *Scherbaum and Sato*, 1991; *Obara and Sato*, 1995] mentioned that the frequency independence of envelope broadening is the result of a Gaussian ACF. However, our result indicates that the frequency independence is not proper to the Gaussian ACF random media, and the envelope broadening becomes independent of frequency even for von Kármán-type random media when short-wavelength components are poor as $\kappa \approx 1.0$.

2.2.4. Contribution of intrinsic absorption and large-angle scattering. [14] In the model we developed above, we have neglected attenuation due to intrinsic absorption and large-angle scattering due to small-scale inhomogeneity. Large-angle scattering works mainly as attenuation in early part of envelopes. To include the attenuation due to large-angle scattering and also intrinsic absorption, we phenomenologically multiply exp $(-bt)$ to the ISD $\hat{I}_0$ as

$$\hat{I}_0(r, t; \omega_c)e^{-bt}, \tag{30}$$

where the relation between attenuation coefficient b and quality factor Q is

$$b = 2\pi f Q^{-1}. \tag{31}$$

For frequencies higher than 1 Hz we assume that b takes a constant value, since Q for S waves is nearly proportional to wave frequency f in the lithosphere [*Sato*, 1984]. Figure 9 shows the ISD at $r_0 = 150$ km in the 6-Hz band for different values of b. Each envelope, normalized by the maximum amplitude, is calculated for $\kappa = 0.5$, $\varepsilon = 0.05$, $a = 5$ km, $V_0 = 4$ km/s. Figure 9 shows that the envelope duration decreases with increasing attenuation (large b) because amplitudes attenuate more rapidly with increasing lapse time.

3. Estimation of the Power Spectra of Random Inhomogeneity

[15] For random media having rich short-wavelength components our model would fail to predict the later part of envelope, or

Table 2. List of Coefficients A_q and B_q in Equation (32) for 0.5 s $< t_q <$ 30 s

b	A_q	B_q
	$p = 1.2$	
0	−0.222	1
0.045	−0.180	0.858
0.09	−0.144	0.752
0.18	−0.101	0.620
0.36	−0.153	0.581
	$p = 1.4$	
0	−0.132	1
0.045	−0.103	0.872
0.09	−0.088	0.790
0.18	−0.057	0.662
0.36	−0.104	0.624
	$p = 1.6$	
0	−0.070	1
0.045	−0.058	0.901
0.09	−0.052	0.829
0.18	−0.016	0.705
0.36	−0.049	0.650
	$p = 1.8$	
0	−0.022	1
0.045	−0.011	0.907
0.09	−0.013	0.855
0.18	−0.005	0.754
0.36	−0.026	0.684
	$p = 2.0$	
0	0. 016	1
0.045	0.022	0.925
0.09	0.025	0.862
0.18	0.026	0.781
0.36	0.007	0.711

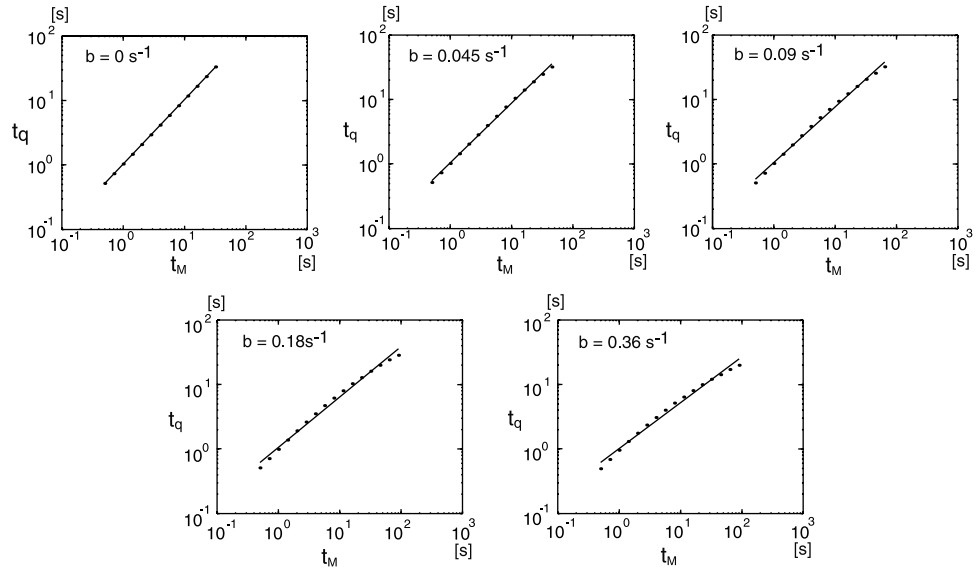

Figure 11. Plots of envelope duration t_q (dots) against characteristic time t_M in the case $p = 2$ for various attenuation coefficients b. The solid line is the regression line given by equation (32).

coda, because the parabolic approximation neglect large-angle scattering. Therefore we will focus on the early part of envelope characterized by its duration as follows. The duration t_q is defined as the time lag between the onset time and the time when RMS envelope decays to the half of the maximum amplitude (Figure 10). That is, the ISD decays to the quarter of the maximum peak value. The duration can be used as a measure of inhomogeneity from recorded wave traces. First, we show a theoretical relation between t_q value and the inhomogeneity parameters, and then we develop a method for estimating the inhomogeneity from measured t_q values of S wave seismogram envelopes of small earthquakes.

3.1. Relation Between Envelope Duration and Parameters Characterizing Random Media

[16] We plot t_q against t_M from the ISD numerically simulated for a given set of b and p values. Assuming

$$\log t_q = A_q(p,b) + B_q(p,b)\log t_M, \tag{32}$$

we estimate A_q and B_q values by using the least squares method for different sets of b and p values in the t_q range from 0.5 to 30 s (see Table 2). For examples, plots for the cases of $p = 2$ for various b values are shown in Figure 11. For small b values, the relation between t_q and t_M is well represented by equation (32) for a wide range of t_q. Equation (32) will provide a simple relation between t_q and random media parameters as follows.

[17] Substituting t_M of equation (24) into (32), we get a relation between t_q and parameters characterizing random media:

$$\log t_q = B_{qr}(p,b)\log r_0 + B_{qf}(p,b)\log f + B_q(p,b)D(p,\varepsilon,a) + A_q(p,b), \tag{33}$$

where coefficients are

$$B_{qr}(p,b) = B_q(p,b)\frac{p+2}{p}, \qquad B_{qf}(p,b) = B_q(p,b)\frac{-2p+4}{p},$$

$$D(p,\varepsilon,a) = \log\left[\frac{C[\kappa(p)]^{\frac{2}{p}}}{2}(2\pi)^{\frac{-2p+4}{p}}V_0^{\frac{p-4}{p}}\left(\varepsilon^{\frac{2}{p-1}}a^{-1}\right)^{\frac{2p-2}{p}}\right]. \tag{34}$$

In the following, we use the dimension of each parameter as follows: r_0 in km, f in Hz, V_0 in km s^{-1}, a in km, and b in s^{-1}. From equation (34) we can get a relation between B_{qr} and B_{qf} for various b and $p(\kappa)$ values as plotted by fine dashed lines in Figure 12. It shows that B_{qr} values, which represent the dependence of t_q on r_0, decrease with increasing b values, and B_{qf} values, which represent the dependence of t_q on f, decrease with increasing $p(\kappa)$ values. In Figure 13 we plot t_q against r_0 for several sets of b and f values as examples for the case of $V_0 = 4$ km s^{-1}, $a = 5$ km, $\varepsilon = 0.05$, and $\kappa = 0.3$. The gradient B_{qr} becomes smaller with increasing

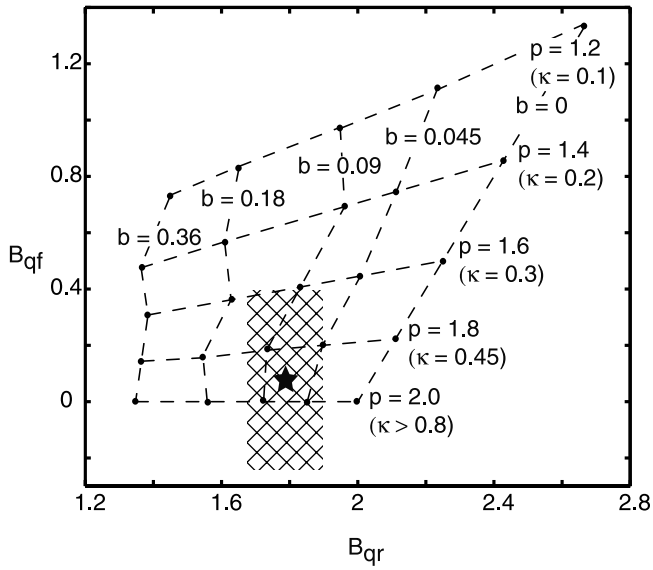

Figure 12. Dashed lines show the relation between B_{qr} and B_{qf} for various b and $p(\kappa)$ values numerically calculated. Star indicates the average observed values in northeastern Honshu, Japan, $\bar{B}_{qr}^{\text{obs}} = 1.79$ and $\bar{B}_{qf}^{\text{obs}} = 0.08$. The hatched area corresponds to the range evaluated from the square root of variances, $1.66 < B_{qr} < 1.89$ and $-0.24 < B_{qf} < 0.40$.

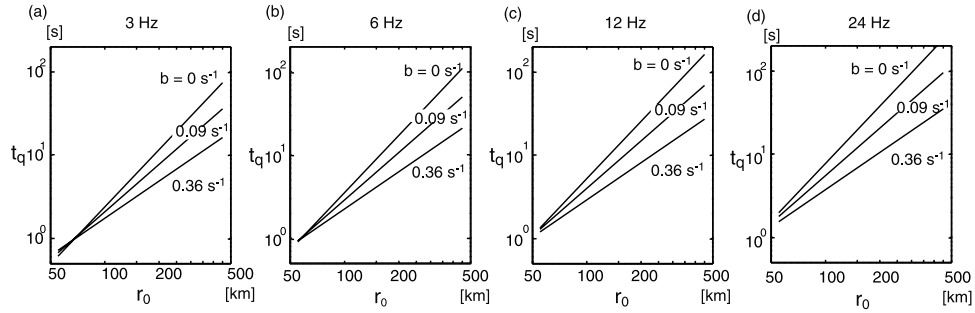

Figure 13. Plots of t_q against r_0 for different values of b for $V_0 = 4$ km s^{-1}, $a = 5$ km, $\varepsilon = 0.05$, $\kappa = 0.3$: (a) $f = 3$ Hz, (b) $f = 6$ Hz, (c) $f = 12$ Hz, and (d) $f = 24$ Hz.

attenuation coefficient b for the same frequency band. The duration t_q becomes larger with increasing frequency for the same b value.

3.2. Estimation of Random Inhomogeneity Parameters From the Measurements of t_q Values

[18] Considering the travel distance dependence and the frequency dependence of envelope durations, we estimate the parameters of the random media as follows. At step 1 we investigate how t_q depends on r_0. Plotting t_q values against hypocentral distance r_0 for many events in each wave frequency band, we get the best fit regression line:

$$\log t_q = A_{qf}^{\mathrm{obs}} + B_{qf}^{\mathrm{obs}} \log r_0. \tag{35}$$

We calculate $\bar{B}_{qf}^{\mathrm{obs}}$ by averaging B_{qf}^{obs} over all frequency bands. At step 2 we investigate how t_q values depend on frequency f. Plotting t_q values against f for each event, we get the best fit regression line:

$$\log t_q = A_{qf}^{\mathrm{obs}} + B_{qf}^{\mathrm{obs}} \log f. \tag{36}$$

We calculate $\bar{B}_{qf}^{\mathrm{obs}}$ by averaging B_{qr}^{obs} over all events. At step 3 we estimate parameters b and p from $\bar{B}_{qr}^{\mathrm{obs}}$ and $\bar{B}_{qf}^{\mathrm{obs}}$ using the theoretical relation between B_{qr} and B_{qf} in Figure 12. Then the order κ is estimated from p value using the relation in Figure 5. At step 4 we estimate $\varepsilon^{2/(P_{\mathrm{est}}-1)}a^{-1}$, so that the theoretical relation (33) agrees with the observed regression line (35) where p_{est} is the estimated p value in step 3.

4. Analysis of Observed *S* Wave Seismogram Envelopes

4.1. Data

[19] Applying the method developed above to S wave seismograms of small earthquakes, we estimate the PSDF of random inhomogeneity of lithosphere beneath northeastern Honshu, Japan. The data we use are velocity seismograms recorded at the Tsuyama station (TYM) located at northeastern Honshu, Japan (38.66°N, 141.37°E, altitude 100 m) (see Figure 14), where a broadband seismometer STS-2 is installed on hard rock. Seismograms are digitized with the sampling frequency of 80 Hz. We selected events for the analysis by the following criteria: the focal depth is deeper than 35 km to avoid crustal reflections, and the magnitude is from 3 to 5 to satisfy the condition that the source duration time is short enough. Figure 14 shows the hypocenter distribution of 328 earthquakes that we used. Station TYM is shown by a triangle. Hypocenter locations were automatically determined by the Research Center for Prediction of Earthquakes and Volcanic Eruptions, Tohoku University. Hypocentral distances analyzed in this study range from 60 to 400 km.

[20] Velocity seismograms in transverse component are calculated from two horizontal component seismograms. Then we make band-pass-filtered traces for four octave width frequency bands 2–4, 4–8, 8–16, and 16–32 Hz. Squared band-pass-filtered traces are smoothed by applying a moving time window of which the width is one half of the center period of each frequency band. We refer to the square root of these traces as RMS envelopes. Except for studies on backscattered coda waves and well log data in the shallow crust, many researches reported that the correlation distance ranges larger than a 10-km as shown in Figure 1 of *Wu and Aki* [1988]. Therefore we may apply the envelope model developed

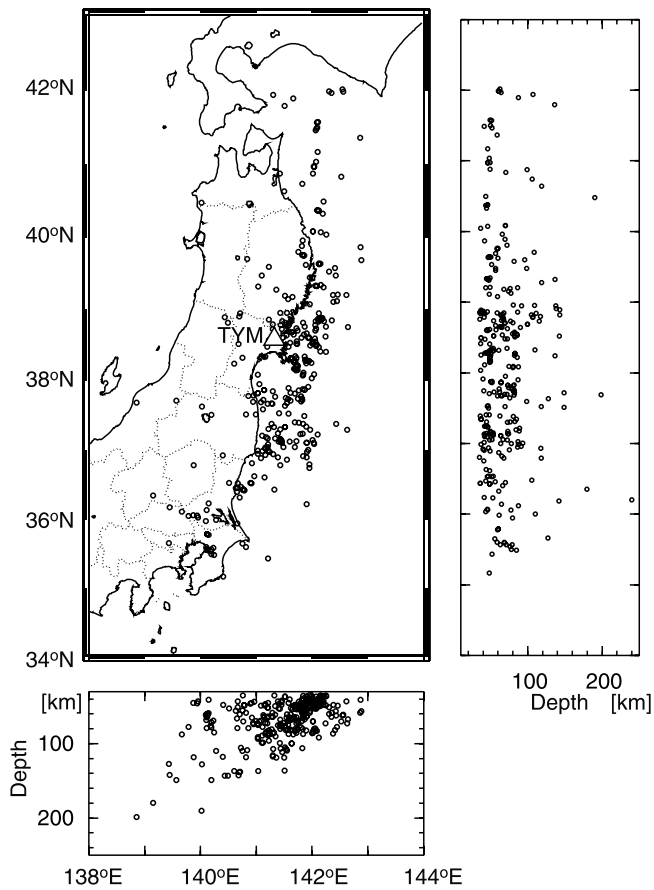

Figure 14. Distribution of 328 small earthquakes that were observed at station TYM (triangle) in northeastern Honshu, Japan. Hypocenter locations were automatically determined by the Research Center for Prediction of Earthquakes and Volcanic Eruptions, Tohoku University.

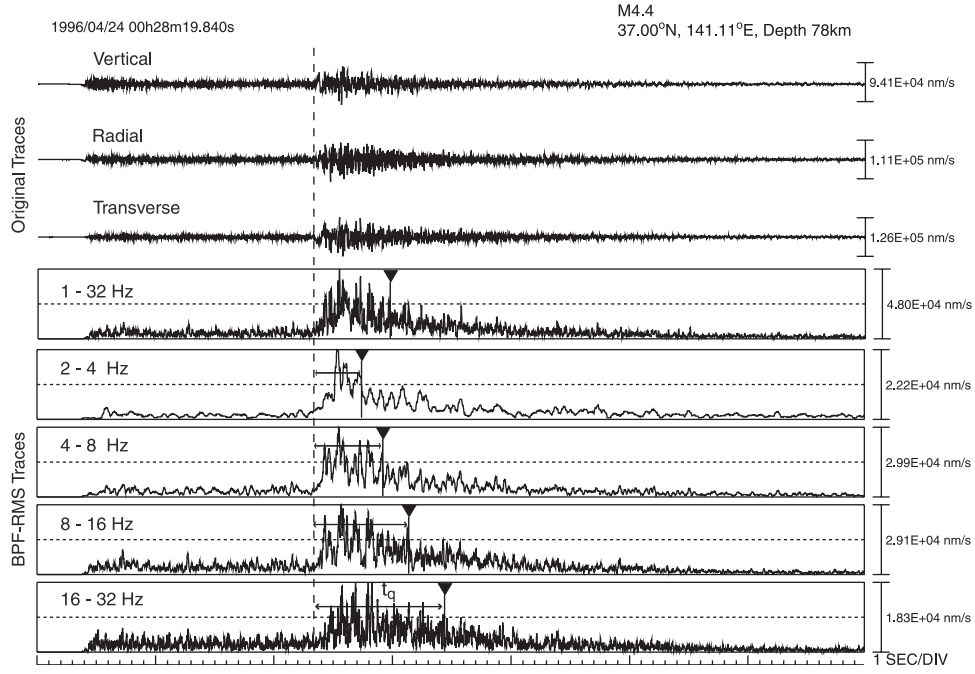

Figure 15. Example of observed seismogram at TYM. Upper three traces are raw velocity seismograms. Lower five traces are transverse component RMS envelopes for frequency bands 1–32, 2– 4, 4–8, 8–16, and 16–32 Hz. The vertical dashed line shows the *S* wave onset time, and each triangle shows the time when RMS amplitude decays to the half of the maximum amplitude for each frequency band.

in this study to *S* waveform data in our frequency ranges. Figure 15 shows an example of records and RMS envelopes of an earthquake (M4.4, 37.00°N, 141.11°E, depth 78 km). Upper three traces are velocity seismograms for vertical, radial, and transverse components. The lower five traces are RMS envelopes of transverse component for frequency bands, 1– 32, 2– 4, 4–8, 8– 16, and 16–32 Hz. Dashed vertical line shows the *S* wave onset time. We manually read the onset time and the time when the RMS envelope decays to the half of the peak value (solid triangle) for each frequency band. The lag time shown by a horizontal arrow represents the envelope duration t_q.

4.2. Results

[21] Following the procedure given in section 3.2, we estimate the von Kármán's parameters and attenuation coefficient.

[22] For step 1, in Figure 16, triangles show plots of observed envelope duration t_q against hypocentral distance r_0 in logarithmic scale for each frequency band, where dashed lines are regression lines. These plots show that t_q increases with increasing r_0 as predicted by our model. Regression coefficients $A_{qr}^{\rm obs}$ and $B_{qr}^{\rm obs}$ and their square root of variances are given at the right bottom of each bin, where STD is the standard deviation of observed data from the regression line. The average value of $B_{qr}^{\rm obs}$ over all frequency bands is $\bar{B}_{qr}^{\rm obs} = 1.79$. We evaluate the range of $B_{qr}^{\rm obs}$ from 1.66 to 1.89, taking the square root of variances for all frequency bands into consideration.

[23] In step 2, we investigate the relation between envelope duration t_q and wave frequency f by calculating regression line (36) for each event. The histogram of $B_{qf}^{\rm obs}$ is plotted in Figure 17. The average value of $B_{qf}^{\rm obs}$ over all events is $\bar{B}_{qf}^{\rm obs} = 0.08$ and its standard deviation is 0.32.

[24] In step 3, we estimate b and κ from $\bar{B}_{qr}^{\rm obs} = 1.79$ and $\bar{B}_{qf}^{\rm obs} = 0.08$. In Figure 12 the star indicates observed $\bar{B}_{qr}^{\rm obs}$ and $\bar{B}_{qf}^{\rm obs}$ values, and the hatched area corresponds to their variation range, $1.66 < \bar{B}_{qr}^{\rm obs} < 1.89$ and $-0.24 < \bar{B}_{qf}^{\rm obs} < 0.40$. From this plot we estimate that $p_{\rm est} = 1.9$ and $b_{\rm est} = 0.06$ s^{-1}. The $p_{\rm est}$ value obtained corresponds to $\kappa_{\rm est} = 0.6$. The ranges of parameters here estimated are roughly $\kappa > 0.3$ and 0.02 s$^{-1} < b < 0.18$ s^{-1}.

[25] In step 4, by using the value $\kappa_{\rm est} = 0.6$ ($p_{\rm est} = 1.9$), we estimate $\varepsilon^{2/(P_{\rm est}-1)}a^{-1}$ as $10^{-3.52}$ [km^{-1}], $10^{-3.61}$ [km^{-1}], $10^{-3.61}$ [km^{-1}], and $10^{-3.53}$ [km^{-1}] for frequency bands 2–4, 4–8, 8–16, and 16–32 Hz, respectively, under the assumption of $V_0 = 4$ km s^{-1}. Taking average over all frequency bands, we get $\varepsilon^{2.2}a^{-1} \approx 10^{-3.57}$ km^{-1}. We cannot delimit the variation range of the parameter $\varepsilon^{2/(P_{\rm est}-1)}a^{-1}$ because the maximum value of κ is not well constrained in our data set.

[26] In summary, best estimates of model parameters are $\varepsilon^{2.2}a^{-1} \approx 10^{-3.57}$ [km^{-1}], $b = 0.06$ [s^{-1}] ($Q_s^{-1} = 0.0095f^{-1}$) and $\kappa = 0.6$. Our method cannot estimate ε and a independently. Considering the approximation range $\varepsilon \ll 1$ and $ka \gg 1$, we can choose ε and a as $(\varepsilon, a) = (0.051, 5\text{ km}), (0.070, 10\text{ km})$, and $(0.096, 20\text{ km})$, for example. Substituting these parameters of von Kármán-type ACF into equation (16), we plot the PSDF (solid bold line) in Figure 18. In that case the asymptote of the PSDF for large wave numbers becomes $P(m) \approx 0.01m^{-4.2}$. Substituting estimated parameters into equation (33), we get the relation between t_q [s], r_0 [km], and f [Hz] as

$$\log t_q = 1.82 \log r_0 + 0.09 \log f - 3.43. \qquad (37)$$

Solid lines in Figure 16 show the theoretical predictions from equation (37). We see that the theoretical predictions and the observed regression lines are in good agreement for all frequency bands.

5. Discussion

[27] In previous studies [*Sato*, 1989; *Scherbaum and Sato*, 1991; *Obara and Sato*, 1995], observed *S* wave envelopes of small earthquakes were analyzed on the basis of a theoretical envelope model for plane waves. In the analysis of this paper we used the theoretical envelope model for spherically outgoing waves

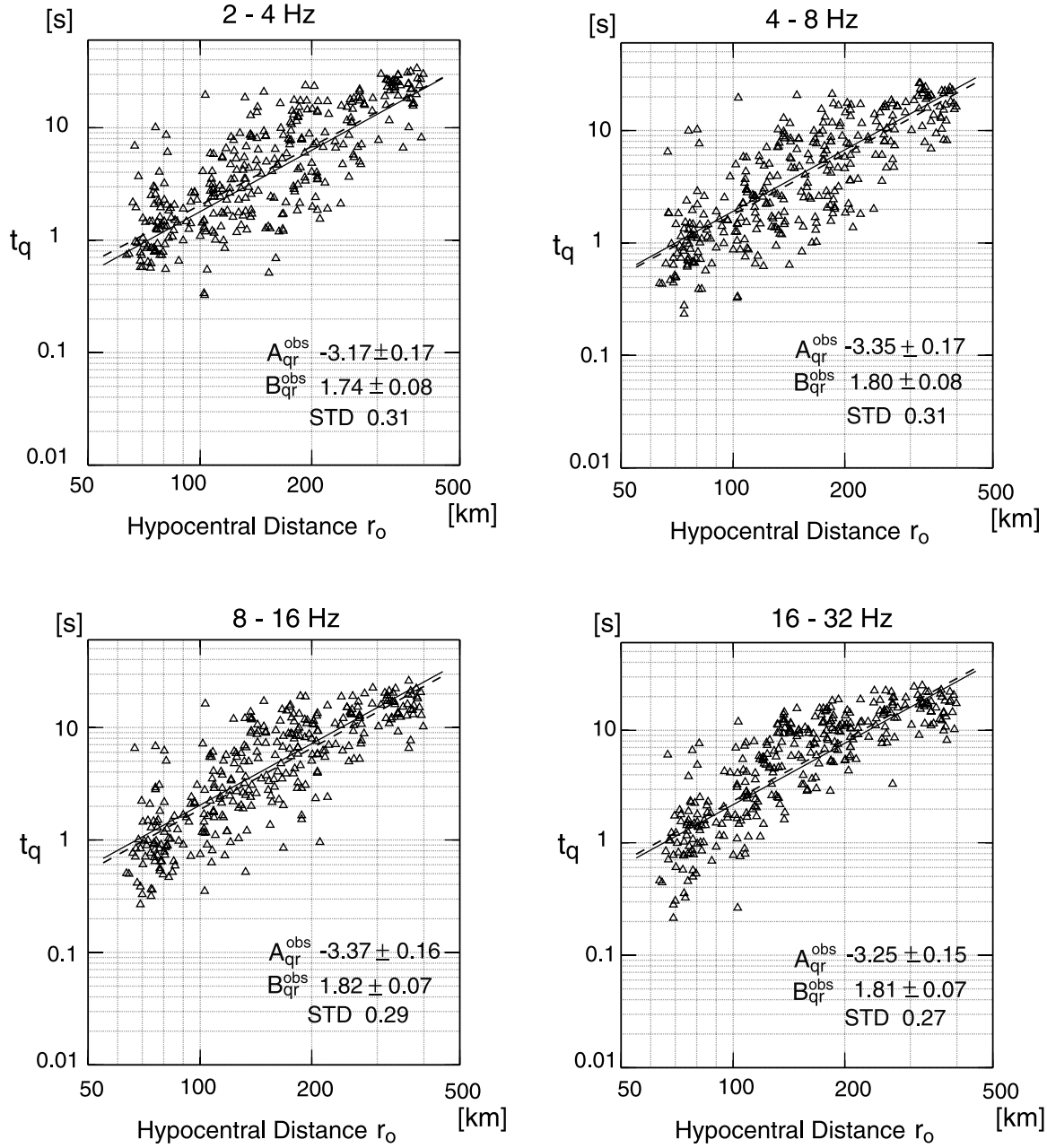

Figure 16. Plots of envelope duration t_q observed (triangle) against hypocentral distance r_0 in logarithmic scale. Dashed lines are regression lines given by equation (35). Regression coefficients A_{qr}^{obs} and B_{qr}^{obs} and standard deviation of observed data from each regression line are shown at the right bottom. Solid lines are theoretically predicted by our model equation (37).

radiated from a point source, which accurately represents a geometrical spreading effect in 3-D media. We examine the difference between the envelopes derived from above two models. The solid curve in Figure 19 shows ISD, which correspond to the MS envelope, of spherically outgoing waves in random media characterized by a Gaussian ACF without attenuation, where the characteristic time $t_M = \sqrt{\pi}\,\varepsilon^2 r_0^2/(2V_0 a)$. The exact derivation is given in Appendix B. The envelope duration $t_q \approx 1.05 t_M$ for ISD of spherically outgoing waves, while $t_q \approx 3.11 t_M$ for ISD of plane waves as drawn by a dashed curve [after *Sato*, 1989]. We may say that the envelope duration of spherically outgoing waves is about 1/3 as long as that of plane waves for a given randomness. It means that the ratio ε^2/a estimated from observed envelope durations based on the plane wave model is systematically underestimated. Such a difference in envelope durations occurs for von Kármán-type random media as well.

[28] Our observational results show that the frequency dependence of envelopes is weak but clear, as shown in Figure 17. In the case of random media having Gaussian ACF, envelopes are independent of wave frequency. Envelopes for von Kármán-type random media change with wave frequency. Observed envelopes, in general, change with wave frequency as was reported by *Obara and Sato* [1995]. They introduce parameter p [*Obara and Sato*, 1995, equation (3)] to generalize an exponential function for the longitudinal integral of ACF to represent the frequency dependence of envelopes; however, they could not derive the corresponding

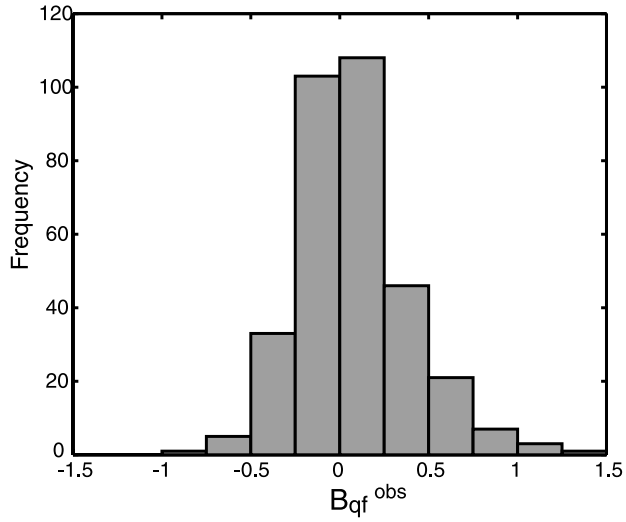

Figure 17. Histogram of B_{qf}^{obs} for all events. The average of B_{qf}^{obs} is 0.08, and its standard deviation is 0.32.

ACF. Our formulation succeeded in relating p value with the order κ of von Kármán-type ACF by using both analytical and numerical simulations (see Figure 5). We note that $p(\kappa)$ and $C(\kappa)$ values estimated in equation (20) slightly vary when we choose a different x range. The variation of these values estimated from different x ranges is the largest around $\kappa = 0.5$. For example, when $\kappa = 0.5$, the p value is 1.80 for the range $10^{-5} \sim 10^{-1}$, while the p value is 1.85 for the range $10^{-3} \sim 10^{-1}$. As examples, we plot RMS envelopes at 8 Hz at distance 150 km for different choices of x range in Figure 20, where we take $V_0 = 4$ km s^{-1}, $\varepsilon = 0.05$, and $a = 5$ km. The scatter of these traces is within 3% of the maximum peak, and

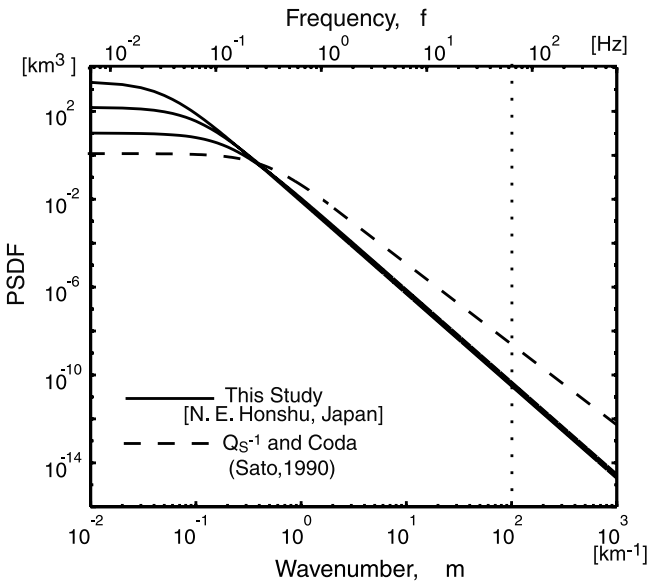

Figure 18. Plots of two von Kármán-type PSDFs estimated in northeastern Honshu, Japan (solid curves): (ε, a, κ) = (0.051, 5 km, 0.6), (0.070, 10 km, 0.6) and (0.096, 20 km, 0.6). Dashed curve shows the PSDF estimated from the frequency dependence of S wave attenuation and coda excitation by *Sato* [1990] ($\varepsilon = 0.08$, a = 2.1 km, $\kappa = 0.35$) as a reference. The vertical dashed line shows twice the maximum wave frequency used in this study.

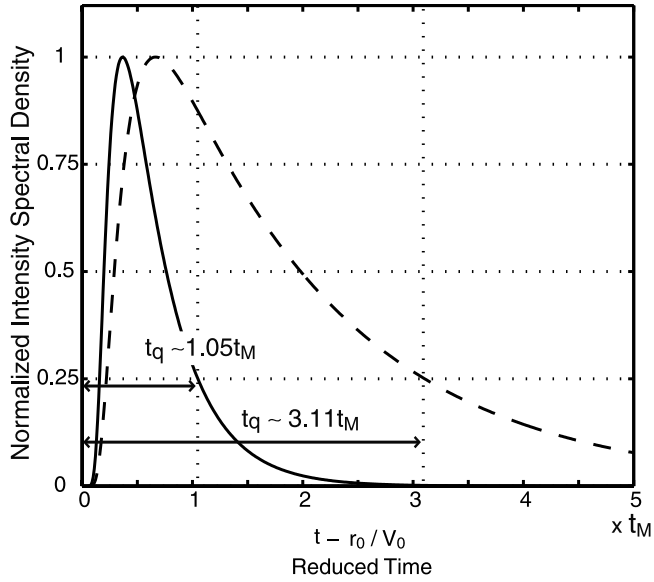

Figure 19. Comparison of the ISD for spherically outgoing waves (solid curve) and that for plane waves (dashed curve) in 3-D random media characterized by a Gaussian ACF without attenuation. Each trace is normalized by the peak value.

the scatter of measured envelope duration t_q is within 10% error. The variation of $p(\kappa)$ and $C(\kappa)$ depending on the x range means that both frequency and travel distance dependencies of envelope broadening slightly vary with travel distance. However, the difference is very small in synthesized envelopes.

[29] We cannot estimate independently parameters ε, a, and κ characterizing PSDF of random media, so that we cannot measure the corner of PSDF curve that corresponds to the reciprocal of the correlation distance. However, the PSDFs in high wave numbers (beyond the corner wave number) take almost the same value for possible combinations of ε and a as shown in Figure 18. That is, we cannot discuss the corner, but

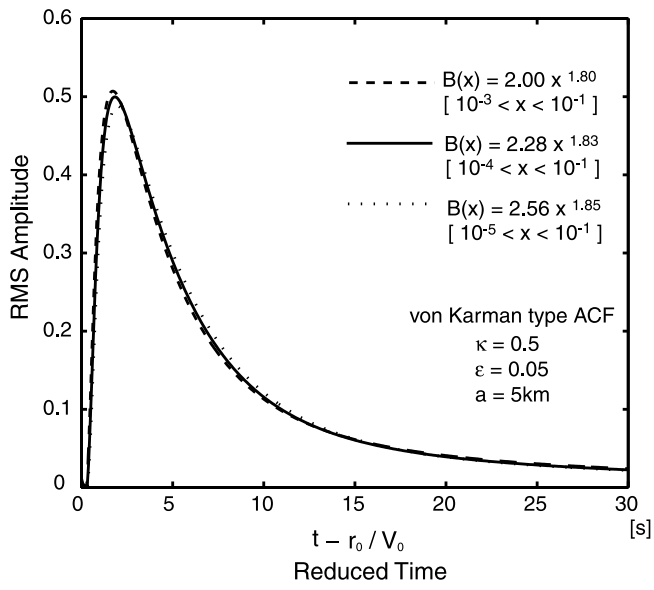

Figure 20. RMS envelopes for different approximation forms of $B(x)$ for $\kappa = 0.5$.

we can discuss the power index and the level of PSDF for high wave numbers. In the Born approximation [see *Sato and Fehler*, 1998] the maximum wave number contributing to scattering amplitudes is twice the incident wave number. The corresponding frequency, which is twice the maximum wave frequency 32 Hz, is shown by the vertical dotted line in Figure 18. Our estimation of the power index is -4.2 ($\kappa = 0.6$) and its variation range is less than -3.6 ($\kappa > 0.3$). *Gusev and Abubakirov* [1996] concluded that the power index of PSDF to be $-3.5 \sim -4$ for explaining qualitative character of observed envelopes. Our result is consistent with their results. There have been a few studies on the estimation of von Kármán's parameters in Japan. From the analysis of frequency dependence of attenuation as scattering loss and coda excitation in the lithosphere, *Sato* [1990] estimated as $\varepsilon = 0.08$, $a = 2.1$ [km], and $\kappa = 0.35$. The estimated PSDFs from these values are also shown by the dashed curve in Figure 18 with our results. Our PSDF contains less short-wavelength components than that of *Sato* [1990]. One reason for the difference might come from the difference of the envelope models: this study assumed multiple forward scattering discarding backscattering and analyzed early part of envelopes, while *Sato* [1990]assumed single scattering of elastic waves and examined frequency dependencies of both attenuation and coda excitation.

[30] In this study, we included the contribution of large-angle scattering only as an attenuation factor in equation (30). Large-angle scattering, however, would cause not only attenuation of the early part of envelope but also later coda excitation. It also has small influence on envelope broadening. We will have to include such a contribution of large-angle scattering because of short-wavelength inhomogeneities in the envelope synthesis in future. We will measure how large-angle scattering contributes to seismogram envelopes in von Kármán-type random media by comparing envelopes of finite difference simulations and those of the Markov approximation method. For more precise modeling of seismogram envelopes from onset to later coda, we need to take not only forward scattering but also large-angle scattering into account. We will be able to establish this task by combining the Markov approximation method and the radiative transfer theory.

6. Conclusion

[31] Using the Markov approximation for the parabolic wave equation, we theoretically derived the MS envelope of spherically outgoing scalar waves radiated from a point source in 3-D random media characterized by a von Kármán-type ACF. This model predicts that the envelope duration is proportional to the second to third power of travel distance and is proportional to the zeroth to second power of wave frequency. When the short-wavelength components are rich in random media, the envelope duration increases with both distance and frequency, while the duration is independent of frequency and is proportional to the square of travel distance when the random inhomogeneity is poor in short-wavelength components. We note that the frequency independence of envelope duration is not a unique consequence of Gaussian ACF, as was suggested in previous studies. For modeling the early part of envelope more realistically, the attenuation coefficient b was phenomenologically introduced as a sum of large-angle scattering loss and intrinsic absorption. On the basis of the theoretical model we established a method for estimating parameters characterizing random media by analyzing the travel distance dependence and wave frequency dependence of envelope durations. Applying this method to *S* wave envelopes of 328 small earthquakes recorded at a single station in northeastern Honshu, Japan, we estimated the PSDF of the random inhomogeneity of the lithosphere for the frequency range from 2 to 32 Hz. A positive correlation between the envelope duration and travel distance was confirmed as predicted, and the parameters are estimated as $\kappa = 0.6$, $\varepsilon^{2.2}a^{-1} \approx 10^{-3.57}$ [km^{-1}], and $b = 0.06$ [s^{-1}] ($Q_s^{-1} = 0.0095f^{-1}$). In that case, the power law portion of the estimated PSDF becomes $P(m) \approx 0.01m^{-4.2}$ [km^3].

Appendix A: Derivation of the Differential Equation for Two-Frequency Mutual Coherence Function

[32] For spherically outgoing scalar waves in 3-D random media the differential equation for two-frequency mutual coherence function (TMCF) was given by *Shishov* [1974]. Here we reproduce the derivation of the differential equation.

[33] Taking an ensemble average of a product of wave fields governed by equation (6), we obtain

$$2i\frac{\partial}{\partial r}\Gamma_2 + \frac{1}{r^2}\left(\frac{\Delta_{\perp 1}}{k_1} - \frac{\Delta_{\perp 2}}{k_2}\right)\Gamma_2 - 2\left\langle (k_1\xi_1 - k_2\xi_2)U_1U_2^* \right\rangle = 0. \tag{A1}$$

Here subscript i means that arguments are (r, θ_i, ϕ_i, ω_i), $\Delta_{\perp i}$ is the angular part of Laplacian for θ_i and ϕ_i, and $k_i = \omega_i/V_0$ for $i = 1$ and 2. The last term can be rewritten by using the longitudinal integral of ACF along the global ray from the source to the receiver $A(r_{\perp d})$ and TMCF:

$$\left\langle (k_1\xi_1 - k_2\xi_2)U_1U_2^* \right\rangle = -\frac{i}{2}\left\{ \left(k_1^2 + k_2^2\right)A(0) - 2k_1k_2A(r_{\perp d}) \right\}\Gamma_2. \tag{A2}$$

The procedure to derive equation (A2) is the same as in the case of plane waves [see *Sato and Fehler*, 1998, equation (8.54)]. Then, equation (A1) is written as

$$2i\frac{\partial}{\partial r}\Gamma_2 + \frac{1}{r^2}\left(\frac{\Delta_{\perp 1}}{k_1} - \frac{\Delta_{\perp 2}}{k_2}\right)\Gamma_2 + i\left\{ \left(k_1^2 + k_2^2\right)A(0) - 2k_1k_2A(r_{\perp d}) \right\}\Gamma_2 = 0. \tag{A3}$$

For scattering within a small angle around the receiver direction, Laplacian for θ_i and ϕ_i can be written as

$$\Delta_{\perp i} \approx \frac{1}{\theta_i}\frac{\partial}{\partial \theta_i}\left(\theta_i \frac{\partial}{\partial \theta_i}\right) + \frac{1}{\theta_i^2}\frac{\partial}{\partial \phi_i^2} \qquad \theta_i \ll 1. \tag{A4}$$

Interpreting θ_i and ϕ_i as polar coordinates on the transverse plane and introducing nondimensional Cartesian coordinates:

$$\eta_{xi} = \theta_i \cos\phi_i, \qquad \eta_{yi} = \theta_i \sin\phi_i, \tag{A5}$$

we rewrite equation (A4) as

$$\Delta_{\perp i} = \frac{\partial^2}{\partial \eta_{xi}^2} + \frac{\partial^2}{\partial \eta_{yi}^2} \qquad \theta_i \ll 1. \tag{A6}$$

Introducing center-of-mass and difference coordinates for two points at $\boldsymbol{\eta}_i = (\eta_{xi}, \eta_{yi})$ on the transverse plane

$$\boldsymbol{\eta}_c = (\boldsymbol{\eta}_1 + \boldsymbol{\eta}_2)/2, \qquad \boldsymbol{\eta}_d = \boldsymbol{\eta}_1 - \boldsymbol{\eta}_2, \tag{A7}$$

we can write equation (A4) as

$$\Delta_{\perp 1} = \frac{1}{4}\nabla_{\perp c} + \nabla_{\perp c}\nabla_{\perp d} + \Delta_{\perp d}, \qquad \Delta_{\perp 2} = \frac{1}{4}\nabla_{\perp c} - \nabla_{\perp c}\nabla_{\perp d} + \Delta_{\perp d}, \tag{A8}$$

where $\nabla_{\perp c}$ and $\Delta_{\perp c}$ are for η_c, and $\nabla_{\perp d}$ and $\Delta_{\perp d}$ are for η_d. Laplacian for η_d is written by using polar coordinates (θ_d, ϕ_d) as

$$\Delta_{\perp d} = \frac{1}{\theta_d}\frac{\partial}{\partial \theta_d}\left(\theta_d \frac{\partial}{\partial \theta_d}\right) + \frac{1}{\theta_d^2}\frac{\partial^2}{\partial \phi_d^2}. \tag{A9}$$

The dimensional difference of two points on the transverse plane $r_{\perp d} = \mathbf{r}_{\perp d}$ is written as

$$r_{\perp d} = r\theta_d. \tag{A10}$$

We note that Γ_2 is independent of center-of-mass coordinate η_c and angle ϕ_d because random media is statistically homogeneous and isotropic: $\Delta_c\Gamma_2 = 0$ and $\partial\Gamma_2/\partial\phi_d = 0$. For the case of quasi-monochromatic waves ($k_1 \approx k_2$), we may write equation (A3) as

$$\frac{\partial}{\partial r}\Gamma_2 + i\frac{k_d}{2k_c^2}\frac{1}{r^2}\left(\frac{\partial^2}{\partial\theta_d^2} + \frac{1}{\theta_d}\frac{\partial}{\partial\theta_d}\right)\Gamma_2 + k_c^2[A(0) - A(r\theta_d)]\Gamma_2 + \frac{k_d^2}{2}A(0)\Gamma_2 = 0, \tag{A11}$$

where $k_c = (k_1 + k_2)/2$ and $k_d = k_1 - k_2$. This is the master equation for TMCF.

Appendix B: MS Envelopes in Random Media Having Gaussian ACF

[34] For spherically outgoing waves in 3-D random media having Gaussian ACF, analytical representation of intensity spectral density (ISD) was first obtained by *Shishov* [1974]. Here we reproduce the derivation in the following. The Gaussian ACF is given by

$$R(x) = \varepsilon^2 \exp\left(-r^2/a^2\right). \tag{B1}$$

Its longitudinal integral A (see equation (9)) becomes

$$A(r_{\perp d}) = \sqrt{\pi}\varepsilon^2 a e^{-r_{\perp d}^2/a^2} \approx \sqrt{\pi}\varepsilon^2 a\left\{1 - (r_{\perp d}/a)^2\right\} \quad r_{\perp d} \ll a. \tag{B2}$$

Substituting equation (B2) in (10), we get the differential equation for ${}_0\Gamma_2$ as

$$\frac{\partial}{\partial r}{}_0\Gamma_2 + i\frac{k_d}{2k_c^2}\frac{1}{r^2}\left(\frac{\partial^2}{\partial\theta_d^2} + \frac{1}{\theta_d}\frac{\partial}{\partial\theta_d}\right){}_0\Gamma_2 + \sqrt{\pi}k_c^2\varepsilon^2 a\left(\frac{r\theta_d}{a}\right)^2{}_0\Gamma_2 = 0 \tag{B3}$$

for $\theta_d \ll 1$. Introducing the characteristic time as

$$t_M = \frac{\sqrt{\pi}\varepsilon^2 a}{2V_0}\left(\frac{r_0}{a}\right)^2, \tag{B4}$$

nondimensional propagation distance τ and the transverse distance χ as given by equation (25), we get a nondimensional form of equation (B3) as

$$\frac{\partial}{\partial\tau}{}_0\Gamma_2 + it_M\omega_d\frac{1}{\tau^2}\left(\frac{\partial}{\partial\chi^2} + \frac{1}{\chi}\frac{\partial}{\partial\chi}\right){}_0\Gamma_2 + \tau^2\chi^2{}_0\Gamma_2 = 0. \tag{B5}$$

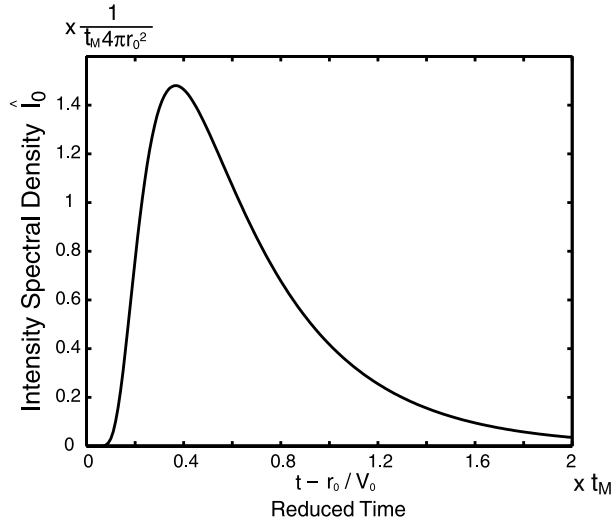

Figure B1. Temporal change in ISD for spherically outgoing waves in random media characterized by a Gaussian ACF without attenuation, where the characteristic time is $t_M = (\sqrt{\pi}\,\varepsilon^2 r^2{}_0)/2V_0 a$.

Writing the solution a priori in the form as

$${}_0\Gamma_2(\chi,\tau) = \frac{e^{\nu(\tau)\tau^2\chi^2}}{w(\tau)} \tag{B6}$$

and substituting it into equation (B5), we get two different equations:

$$\nu' + \frac{2\nu}{\tau} + s_0^2\nu^2 + 1 = 0, \tag{B7}$$

$$s_0^2\nu - \frac{w'}{w} = 0, \tag{B8}$$

where $s_0 = 2e^{i\pi/4}\sqrt{t_M\omega_d}$. Equation (B7) is a Riccati equation. Solutions of these equations are

$$\nu = \frac{1}{s_0}\cot(s_0\tau + c_1) - \frac{1}{s_0^2\tau}, \tag{B9}$$

$$w = \frac{c_2\,\sin(s_0\tau + c_1)}{s_0\tau}. \tag{B10}$$

Under the initial condition (13), we obtain the analytical solution

$${}_0\Gamma_2 = \frac{1}{4\pi}\frac{s_0\tau}{\sin s_0\tau}\exp\left\{\left(\frac{\tau^2}{s_0}\cot s_0\tau - \frac{\tau}{s_0^2}\right)\chi^2\right\}. \tag{B11}$$

Substituting equation (B11) into (12), we obtain the ISD at a distance r_0 as

$$\hat{I}_0(r_0,t;\omega_c) = \frac{1}{2\pi r_0^2}\int_{-\infty}^{\infty}{}_0\Gamma_2(\tau=1,\chi=0;t_M\omega_d)e^{-i\omega_d(t-r_0/V_0)}d\omega_d$$

$$= \frac{1}{2\pi r_0^2}\int_{-\infty}^{\infty}\frac{1}{4\pi}\frac{2e^{i\pi/4}\sqrt{t_M\omega_d}}{\sin\{2e^{i\pi/4}\sqrt{t_M\omega_d}\}}e^{-i\omega_d(t-r_0/V_0)}d\omega_d$$

$$= \frac{1}{4\pi r_0^2} H\left(t - \frac{r_0}{V_0}\right) \frac{\pi^2}{2t_M} \sum_{n=1}^{\infty} (-1)^{n+1} n^2 e^{-\frac{n^2 \pi^2 (t - r_0/V_0)}{4t_M}} \tag{B12}$$

where $H(t)$ is a step function. This analytic representation is given by equation (34) of *Shishov* [1974]. Figure B1 shows the temporal change in the ISD.

[35] **Acknowledgments.** The authors are grateful to J. Haines, J. A. Hudson, and an anonymous Associate Editor for their critical comments. They are very helpful for improving our study. We would like to express sincere thanks to the staff of the Research Center for Prediction of Earthquakes and Volcanic Eruptions, Tohoku University, for providing us with hypocenter data. This study was partially supported by Grant-in-Aid for Scientific Research (C), MEXT, Japan (Project 1260400).

References

Abramowitz, M., and I. A. Stegun, *Handbook of Mathematical Functions with Formulas, Graphs, and Mathematical Tables*, Dover, Mineola, N. Y., 1970.

Aki, K., Scattering of *P* waves under the Montana LASA, *J. Geophys. Res.*, *78*, 1334–1346, 1973.

Aki, K., and B. Chouet, Origin of coda waves: Source, attenuation and scattering effects, *J. Geophys. Res.*, *80*, 3322–3342, 1975.

Capon, J., Characterization of crust and upper mantle structure under LASA as a random medium, *Bull. Seismol. Soc. Am.*, *64*, 235–266, 1974.

Fehler, M., H. Sato, and L.-J. Huang, Envelope broadening of outgoing waves in 2-D random media: A comparison between the Markov approximation and numerical simulations, *Bull. Seismol. Soc. Am.*, *90*, 914–928, 2000.

Flatté, S. M., and R. S. Wu, Small-scale structure in the lithosphere and asthenosphere deduced from arrival time and amplitude fluctuations at NORSAR, *J. Geophys. Res.*, *93*, 6601–6614, 1988.

Gusev, A. A., and I. R. Abubakirov, Simulated envelopes of non-isotropically scattered body waves as compared to observed ones: Another manifestation of fractal heterogeneity, *Geophys. J. Int.*, *127*, 49–60, 1996.

Ishimaru, A., *Wave Propagation and Scattering in Random Media*, 2 vols., Academic, San Diego, Calif., 1978.

Lee, L. C., and J. R. Jokipii, Strong scintillations in astrophysics, II, A theory of temporal broadening of pulses, *Astrophys. J.*, *201*, 532–543, 1975.

Liu, Y. B., and R. S. Wu, A comparison between phase screen, finite difference, and eigenfunction expansion calculations for scalar waves in inhomogeneous media, *Bull. Seismol. Soc. Am.*, *84*, 1154–1168, 1994.

Obara, K., and H. Sato, Regional differences of random inhomogeneities around the volcanic front in the Kanto-Tokai area, Japan, revealed from the broadening of *S* wave seismogram envelopes, *J. Geophys. Res.*, *100*, 2103–2121, 1995.

Press, W. H., S. A. Teukolsky, W. T. Vetterling, and B. P. Flannery, *Numerical Recipes in C*, Cambridge Univ. Press, New York, 1987.

Sato, H., Attenuation and envelope formation of three-component seismograms of small local earthquakes in randomly inhomogeneous lithosphere, *J. Geophys. Res.*, *89*, 1221–1241, 1984.

Sato, H., Broadening of seismogram envelopes in the randomly inhomogeneous lithosphere based on the parabolic approximation: Southeastern Honshu, Japan, *J. Geophys. Res.*, *94*, 17735–17747, 1989.

Sato, H., Unified approach to amplitude attenuation and coda excitation in the randomly inhomogeneous lithosphere, *Pure Appl. Geophys.*, *132*, 93–121, 1990.

Sato, H., and M. Fehler, *Seismic Wave Propagation and Scattering in the Heterogeneous Earth*, AIP Press, New York, 1998.

Scherbaum, F., and H. Sato, Inversion of full seismogram envelopes based on the parabolic approximation: Estimation of randomness and attenuation in southeast Honshu, Japan, *J. Geophys. Res.*, *96*, 2223–2232, 1991.

Shiomi, K., H. Sato, and M. Ohtake, Broad-band power-law spectra of well-log data in Japan, *Geophys. J. Int.*, *130*, 57–64, 1997.

Shishov, V. L., Effect of refraction on scintillation characteristics and average pulsars, *Sov. Astron.*, *17*, 598–602, 1974.

Sreenivasiah, I., A. Ishimaru, and S. T. Hong, Two-frequency mutual coherence function and pulse propagation in a random medium: An analytic solution to the plane wave case, *Radio Sci.*, *11*, 775–778, 1976.

Tatarskii, V. I., *The Effects of the Turbulent Atmosphere on Wave Propagation*, Isr. Program for Sci. Transl., Jerusalem, 1971.

Wu, R. S., and K. Aki, The fractal nature of the inhomogeneities in the lithosphere evidenced from seismic wave scattering, *Pure Appl. Geophys.*, *123*, 805–818, 1985.

Wu, R. S., and K. Aki, Introduction: Seismic wave scattering in three-dimensionally heterogeneous Earth, *Pure Appl. Geophys.*, *128*, 1–6, 1988.

M. Ohtake, T. Saito, and H. Sato, Department of Geophysics, Graduate School of Science, Tohoku University, Aoba-ku, Sendai 980-8578, Japan. (saito@zisin.Geophys.tohoku.ac.jp)

Correction to "Envelope broadening of spherically outgoing waves in three-dimensional random media having power law spectra" by Tatsuhiko Saito, Haruo Sato, and Masakazu Ohtake

Received 27 June 2002; published 25 September 2002.

INDEX TERMS: 9900 Corrections

Citation: Saito T., H. Sato, and M. Ohtake, Correction to "Envelope broadening of spherically outgoing waves in three-dimensional random media having power law spectra" by Tatsuhiko Saito, Haruo Sato, and Masakazu Ohtake, *J. Geophys. Res.*, *107*(B9), 2197, doi:10.1029/2002JB002063, 2002.

[1] In the paper "Envelope broadening of spherically outgoing waves in three-dimensional random media having power law spectra" by Tatsuhiko Saito, Haruo Sato, and Masakazu Ohtake (*Journal of Geophysical Research*, *107*(B5), 10.1029/2001JB000264, 2002), equations (11), (22a), (22b), (35), (36) and (B12) contained typographical errors.

1. Equation (11)

[2] On the right-hand side of the second part of equation (11), θ_d is mistyped and the integration symbol should be corrected as follows:

$$\begin{aligned} I_0(r,t) &\equiv \langle u(r,\mathbf{r}_\perp,t)u^*(r,\mathbf{r}_\perp,t)\rangle \\ &= \frac{1}{(2\pi)^2}\frac{1}{r^2}\int_{-\infty}^{\infty}\int_{-\infty}^{\infty} d\omega_d \quad d\omega_c \\ &\quad \cdot {}_0\Gamma_2(\theta_d = 0, r, \omega_d, \omega_c)e^{-i\omega_d(t-r/V_0)} \\ &= \frac{1}{2\pi}\int_{-\infty}^{\infty} d\omega_c \hat{I}_0(r,t;\omega_c). \end{aligned} \tag{11}$$

2. Equations (22a) and (22b)

[3] The corrected version of equations (22a) and (22b) is as follows:

$$B\left(\frac{r_{\perp d}}{a};\kappa\right) \approx \frac{2^{-\kappa+\frac{1}{2}}\pi^{\frac{3}{2}}}{\Gamma(\kappa)\cos\kappa\pi}\left\{\frac{2^{-\kappa-\frac{1}{2}}}{\Gamma(3/2+\kappa)}\left(\frac{r_{\perp d}}{a}\right)^{2\kappa+1}\right\} \tag{22a}$$

$$B\left(\frac{r_{\perp d}}{a};\kappa\right) \approx \frac{2^{-\kappa+\frac{1}{2}}\pi^{\frac{3}{2}}}{\Gamma(\kappa)\cos\kappa\pi}\left\{\frac{-2^{\kappa-\frac{3}{2}}}{\Gamma(3/2-\kappa)}\left(\frac{r_{\perp d}}{a}\right)^{2}\right\} \tag{22b}$$

3. Equations (35) and (36)

[4] The correct version of equations (35), (36), and terms in the following text is as follows:

$$\log t_q = A_{qr}^{\mathrm{obs}} + B_{qr}^{\mathrm{obs}} \log r_0. \tag{35}$$

We calculate $\overline{B}_{qr}^{\mathrm{obs}}$ by averaging B_{qr}^{obs} over all frequency bands. At step 2 we investigate how t_q values depend on frequency f. Plotting t_q values against f for each event, we get the best fit regression line,

$$\log t_q = A_{qf}^{obs} + B_{qf}^{obs} \log f. \tag{36}$$

We calculate $\overline{B}_{qf}^{\mathrm{obs}}$ by averaging B_{qf}^{obs} over all events. At step 3 we estimate parameters b and p from $\overline{B}_{qr}^{\mathrm{obs}}$ and $\overline{B}_{qf}^{\mathrm{obs}}$ using the theoretical relation between B_{qr} and B_{qf} in Figure 12.

4. Equation (B12)

[5] On the right-hand side of the third part of equation (B12) the superscript of e is wrong. The correct version is as follows:

$$\begin{aligned} &\hat{I}_0(r_0,t;\omega_c) \\ &= \frac{1}{2\pi r_0^2}\int_{-\infty}^{\infty} {}_0\Gamma_2(\tau=1,\chi=0;t_M\omega_d)\; e^{-i\omega_d(t-r_0/V_0)}d\omega_d \\ &= \frac{1}{2\pi r_0^2}\int_{-\infty}^{\infty} \frac{1}{4\pi}\frac{2e^{i\pi/4}\sqrt{t_M\omega_d}}{\sin\{2e^{i\pi/4}\sqrt{t_M\omega_d}\}}e^{-i\omega_d(t-r_0/V_0)}d\omega_d \\ &= \frac{1}{4\pi r_0^2}H\left(t-\frac{r_0}{V_0}\right)\frac{\pi^2}{2t_M}\sum_{n=1}^{\infty}(-1)^{n+1}n^2\, e^{-\frac{n^2\pi^2(t-r_0/V_0)}{4t_M}} \end{aligned} \tag{B12}$$

0148-0227/02/2002JB002063$09.00